Barotropic tidal and wind-driven larval transport in the vicinity of a barrier island inlet

RICHARD A. LUETTICH JR,[1] JAMES L. HENCH,[1] CRYSTAL W. FULCHER,[1] FRANCISCO E. WERNER,[2] BRIAN O. BLANTON[2] AND JAMES H. CHURCHILL[3]

[1]*University of North Carolina at Chapel Hill, Institute of Marine Sciences, 3431 Arendell Street, Morehead City, NC 28557, USA*
[2]*University of North Carolina at Chapel Hill, Department of Marine Sciences, Box 3300, Chapel Hill, NC 27599-3300, USA*
[3]*Woods Hole Oceanographic Institution, Clark Laboratory, Woods Hole, MA 02543, USA*

ABSTRACT

Fish species such as Atlantic menhaden (*Brevoortia tyrannus*) must often transit relatively small barrier island inlets to move from their continental shelf spawning grounds to estuarine nurseries, where they spend their juvenile phase. Physical transport through these inlets is strongly influenced by tides, winds, local geometry and bathymetry, and can be very different from that occurring on the shelf. In March 1996, an extensive multidisciplinary field experiment was conducted to identify larval transport pathways in the vicinity of Beaufort Inlet, NC (Blanton *et al.*, 1999; Churchill *et al.*, 1999; Forward *et al.*, 1999). One of the most interesting results from the field study was significant spatial inhomogeneity in the larval catches (Forward *et al.*, 1999).

This paper describes a computer modelling study of tidal and wind-driven circulation and accompanying larval transport characteristics in the vicinity of Beaufort Inlet. Primary conclusions are as follows: (i) tidal currents are quite effective at creating net larval transport into the inlet; (ii) in the absence of wind forcing, to explain the spatial distribution of larval catches observed in the field experiment, the primary source of larvae must have been to the east of the inlet; (iii) the spring/neap cycle accounts for a variation of approximately 40% in larvae ingress; (iv) only a few wind directions enhance larvae ingress over the case of purely tidal forcing—wind blowing toward the north enhances ingress at the surface, and winds blowing toward the south and the east enhance ingress at the bottom; (v) if larvae are evenly distributed in space outside the inlet, then strong east wind (such as 10 m s^{-1}) can cause larvae to move through the inlet in a way that is consistent with the larval catches in the field experiment. However, local wind records revealed that no significant eastward-blowing winds occurred during or immediately preceding the field experiment.

Key words: larval transport, inlet studies, modelling, circulation

INTRODUCTION

The life cycle of fish species such as Atlantic menhaden (*Brevoortia tyrannus*) that spawn in continental shelf waters and spend their juvenile phase in estuarine nursery grounds depends critically on physical processes that transport larval fish from spawning areas to juvenile nurseries (Miller *et al.*, 1984). In the South Atlantic Bight, transport on the mid-to inner continental shelf is primarily wind driven (Werner *et al.*, 1999), with additional influences from Gulf Stream intrusions (Stegmann *et al.*, 1999). However, in most cases, to reach estuarine nursery areas, larvae must find and transit relatively small barrier island inlets. Physical transport through these inlets is strongly influenced by tides, local geometry and bathymetry, so is very different from that occurring on the shelf. Thus, a dedicated effort to understand this phase of larval transport is critical. In addition, since many inlets are modified by dredging and jetty structures to maintain navigability, it is important to understand inlet transport as a basis for assessing the implications of these actions.

Barotropic tidal circulation patterns on the seaward side of an idealized, symmetric inlet are reasonably well established (see, for example, Zimmerman, 1981; Mehta, 1988; Oertel, 1988). On ebb tide, a boundary-separated jet forms that preferentially transports water out of the estuary in line with the inlet centre. In contrast, on flood tide, the inflow is uniformly distributed in a convergent pattern toward the inlet.

Correspondence: Dr Rick Luettich, UNC Institute of Marine Sciences, 3431 Arendell Street, Morehead City, NC 28557, USA.
Received for publication 15 October 1998
Accepted for publication 1 July 1999

© 1999 Blackwell Science Ltd.

The difference between the ebb and flood patterns sets up a steady tidal residual circulation that is offshore in the inlet centre, towards the inlet near shore, and contains counterrotating eddies on either side of the offshore flow. (Looking in the offshore direction from the inlet mouth, these eddies rotate counterclockwise to the left of the inlet and clockwise to the right of the inlet.) In the Northern Hemisphere, the clockwise eddy is generally stronger than the counterclockwise eddy, owing to the influence of the Earth's rotation. The strength of both eddies is enhanced by offshore sloping topography (Chao, 1990). On the landward side of an inlet, marsh systems, shoals and/or the shoreline often prevent a similar pattern from forming and largely dominate the circulation patterns that occur there.

Baroclinic effects associated with fresh-water discharge have also been studied in idealized inlets. Fresh-water discharge superimposes estuarine-like circulation (seaward flowing buoyant water overriding shoreward flowing dense water) over the barotropic tidal circulation. During ebb tide, buoyant water flows over denser shelf water, creating a stably stratified water column and a plume outside of the inlet. Owing to the Earth's rotation, in the Northern Hemisphere, plumes are characterized by clockwise circulation that enhances the strength of the clockwise residual eddy and diminishes the strength of the counterclockwise residual eddy near the surface (Chao, 1990; Kapolnai *et al.*, 1996; Wheless and Valle-Levinson, 1996). A weaker counterclockwise circulation develops under the plume and a buoyant surface coastal current that moves away from the inlet to the right (in the Northern Hemisphere) may also form (Chao, 1990). During flood tide, stratification is largely destroyed as denser shelf water is transported through the inlet (Wheless and Valle-Levinson, 1996).

Past inferences about larval transport through tidal inlets and adjacent estuaries have been drawn from the relationship between the vertical position of larvae in the water column and the phase of the tidal cycle (Hill, 1991; Smith and Stoner, 1993; DeVries *et al.*, 1994; Chen *et al.*, 1997; Power, 1997), considerations of subtidal physical processes, such as buoyancy-induced circulation or gradients in wind-driven water level set up (Pietrafesa and Janowitz, 1988), and the potential for larvae to remain entrapped in gyres or other areas of slow flow within an estuary (Fore and Baxter, 1972; Trinast, 1975). However, there has been little work on net larval transport associated with tidal dispersion, as described by Zimmerman (1976), which results from the interaction between a spatially varying oscillatory current (such as a tide near irregular bathymetry) and a spatially varying residual current (such as a tidal or wind-driven residual). This mechanism can account for significant net transport when geometric and topographic variability is large over spatial scales less than a tidal excursion length (Geyer and Signell, 1992), as can be expected near tidal inlets. Perhaps the main reason why tidal dispersion has not been widely considered in larval studies is because it requires detailed information about the horizontal structure of the flow. This information is most readily obtained from numerical circulation models (see, for example, Seabergh, 1988; Geyer and Signell, 1992), the development of which can be quite challenging in the highly complex geometry and topography that typically surround a tidal inlet.

In the present study, we consider larval transport in the vicinity of Beaufort Inlet, North Carolina (Fig. 1). The inlet is approximately 1 km wide and connects a complicated estuarine system to Onslow Bay and the South Atlantic Bight. Immediately inside the inlet,

Figure 1. Location map of the Beaufort Inlet study area.

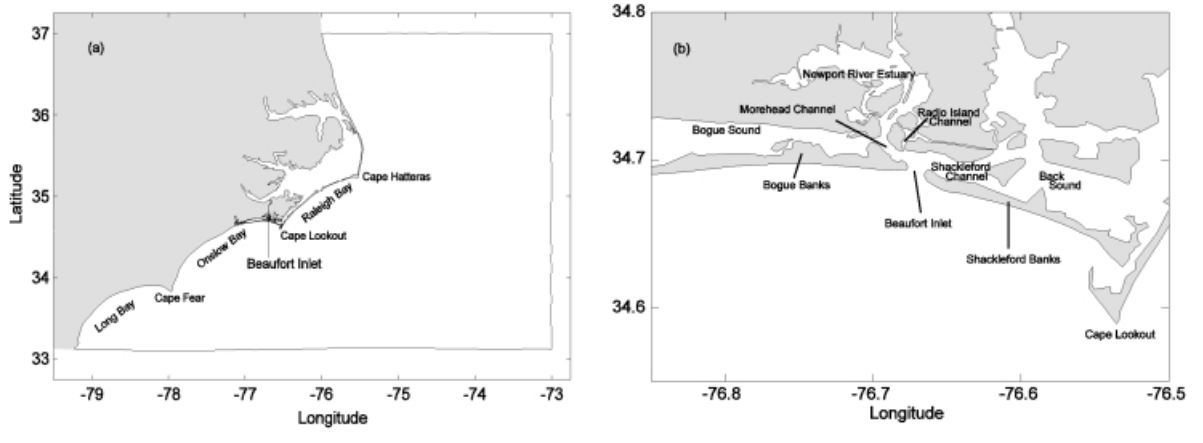

flow is directed through the Morehead Channel, the Radio Island Channel or the Shackleford Channel. Habitat quality is dramatically different in the waters upstream of these channels, as the Morehead Channel connects to the port of Morehead City, the highly developed Bogue Sound and the relatively undeveloped Newport River Estuary; the Radio Island Channel connects to the fully developed waterfront of Beaufort, NC, and the Newport River Estuary; the Shackleford Channel connects to relatively pristine, high-quality nursery areas.

Flow near the inlet is dominated by the semidiurnal, M_2 tide with additional episodic contributions from wind and fresh-water forcing (Klavans, 1983; Logan, 1995). Beaufort Inlet was the site of a multidisciplinary, larval transport field experiment conducted during two consecutive neap tides in March 1996. Physical data from this experiment (Blanton *et al.*, 1999) indicate that fresh-water discharge was significant during the first period (salinity ranged from 20 to 34 psu over the tidal cycle) but much less during the second period (salinity ranged from 32.5 to 34.5 psu over the tidal cycle). During both periods, the water column was vertically well-mixed both in the inlet mouth and in the channels shoreward of the inlet, through virtually the entire tidal cycle. Despite the difference in fresh-water discharge, patterns of larval catches inside the inlet remained remarkably consistent between the two periods (Forward *et al.*, 1999). The spatial scales of the inlet, the presence of a well-mixed water column and the apparent insensitivity of larval catches to buoyant discharge encouraged us to focus initial modelling efforts on the barotropic component of the tidal and wind-driven circulation. Specifically, we have sought to (i) understand basic tidal circulation and tidal dispersion in the vicinity of Beaufort Inlet; (ii) to provide insight into the field observation that an order of magnitude more larvae enter the inlet and move eastward through the Shackleford Channel than move westward through the dredged Morehead Channel (Forward *et al.*, 1999); and (iii) to assess the role of wind forcing vs. tidal forcing in determining larvae ingress through Beaufort Inlet.

BEAUFORT INLET CIRCULATION

Barotropic circulation in Beaufort Inlet was computed using two complementary numerical hydrodynamic models. Tidal circulation was computed using the depth-integrated version of the ADCIRC model (Luettich *et al.*, 1992), while wind-driven circulation was computed in three dimensions using the FUNDY5 model (Lynch *et al.*, 1992).

Both ADCIRC and FUNDY5 utilize the finite element method on linear triangles for their spatial discretization and have been run on a grid (Figs 2 and 3) that stretches from approximately the North Carolina–Virginia border to the South Carolina–Georgia border. The grid extends from the deep ocean (more than 5000 m deep) to estuarine tidal flats that wetted and dried (in the tidal simulations only), and has element sizes ranging from approximately 25 km in deep water to 25 m near shore.

ADCIRC is a fully nonlinear, time-stepping model that accurately generates overtides and compound tides in strongly nonlinear tidal flows (Grenier *et al.*, 1995). The two-dimensional assumption is appropriate for energetic tidal flows where the water column remains well mixed and the water column depth is small compared with the Ekman depth. However, a two-dimensional model is not appropriate for wind-driven flows in shallow enclosed or semi-enclosed areas, where

Figure 2. Finite element grid used for the Beaufort Inlet modelling study.

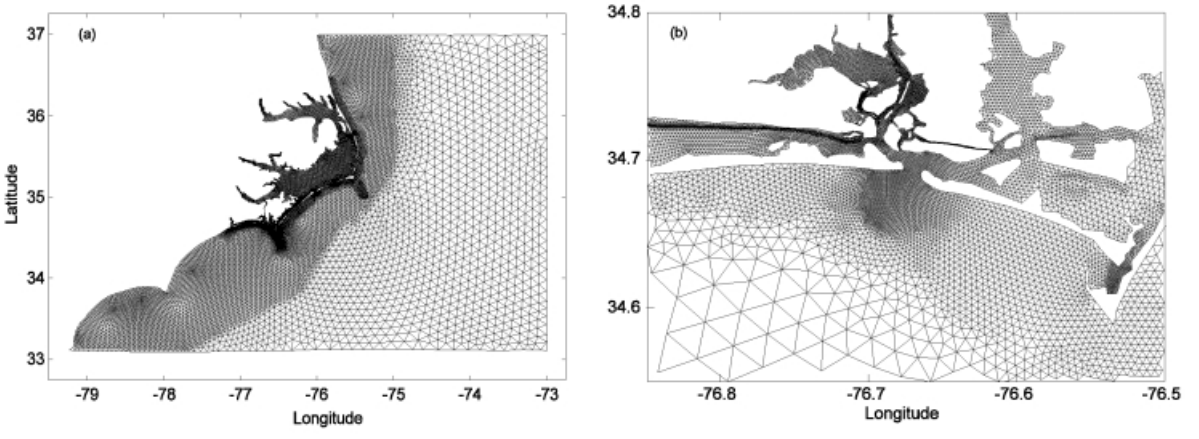

Figure 3. Model bathymetry used in the Beaufort Inlet study. Depth contours are in metres.

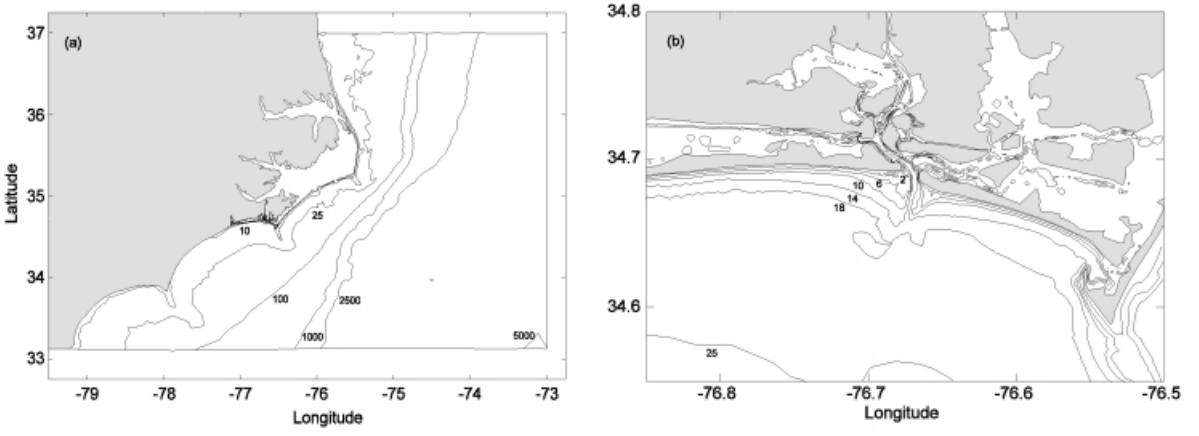

the presence of land can force an upwind circulation at depth that opposes the generally down-wind circulation at the water surface. Therefore, the FUNDY5 model, which provides a harmonic in time solution to the linearized, three-dimensional equations of motion, was used to describe the wind-driven current fields.

Tidal model results

The ADCIRC model was forced using the five primary astronomical constituents: M_2, S_2, N_2, K_1 and O_1. Forcing was applied throughout the domain using the direct tide producing tidal potential terms, and along open boundaries using elevations extracted from the FES95.2 global tidal database (Le Provost *et al.*, 1998). A hybrid bottom friction formulation was used that approached a quadratic relationship with a friction coefficient of 0.0025 in water deeper than 1 m, and a Manning relationship (Manning's $n = 0.016$) in shallower water. Based on preliminary model runs, a spatially constant lateral viscosity of 2 $m^2\ s^{-1}$ was used to maintain numerical stability. While some noise appears in the residual velocity field at a few locations, this was considered to be preferable to the reduction in lateral shear that resulted from using a significantly larger value. The model time step (Courant number limited) was 5 s. The model was spun-up from rest for 10 days, and the subsequent 30 days were harmonically analysed at all grid points within the domain for the five astronomical constituents as well as for the steady residual component and 24 nonlinearly generated compound tides and overtides. As described in the following, the model results were in good agreement with available observational data, so no calibration of the model was attempted (such as by adjusting the open boundary conditions, water depths or bottom friction coefficients).

The amplitude and Greenwich phase of the dominant semidiurnal (M_2) and diurnal (K_1) tidal constituents are shown in Fig. 4. The semidiurnal tide on the shelf is a co-oscillation between the shelf waters and the Atlantic Ocean, and arrives nearly in phase along much of the US east coast. On entering the inlet, it is strongly influenced by bottom friction, owing to the shallow water depths and high current velocities, and is quickly attenuated (Fig. 4(a)) and slowed (Fig. 4(b)) as it propagates into the sounds. The diurnal tide on the shelf is a southward propagating wave that attenuates more slowly inside the estuary (Figs 4(c) and 4(d)), owing to its lower velocity and the resulting reduced frictional influence (Grenier *et al.*, 1995).

Modelled vertically integrated tidal velocities (the full model response to the five astronomical constituent forcing) for the area around Beaufort Inlet are shown at four phases of the tide in Fig. 5. Velocities reach approximately 1 m s^{-1} at maximum flood and ebb in the inlet throat (Figs 5(b) and 5(d)). The ebb flow exits the inlet with a jet-like structure, while the flood flow is fairly uniformly distributed in space outside the inlet. It is clear that any similar pattern inside the inlet is disrupted by the islands and shoreline. Near slack before ebb (Fig. 5(a)) and slack before flood (Fig. 5(c)), the tide can be seen to turn in the Morehead Channel (west of the inlet) earlier than it turns in the Shackleford Channel (east of the inlet). The model indicates a difference of approximately 45 min between the time of slack tide in these two channels, which corresponds closely to differences in the time of slack tide measured during the larval transport field experiments conducted during March 1996 (Blanton *et al.*, 1999; Churchill *et al.*, 1999). The velocity field at slack before flood (Fig. 5(c)) also suggests that initial flooding of the inlet consists of 'new' ocean water travelling west along Shackleford Banks entering the eastern side of

Figure 4. Tidal elevation amplitude (metres) and Greenwich phase (degrees) of the largest semidiurnal (M_2) and diurnal (K_1) tidal constituents for the area around Beaufort Inlet.

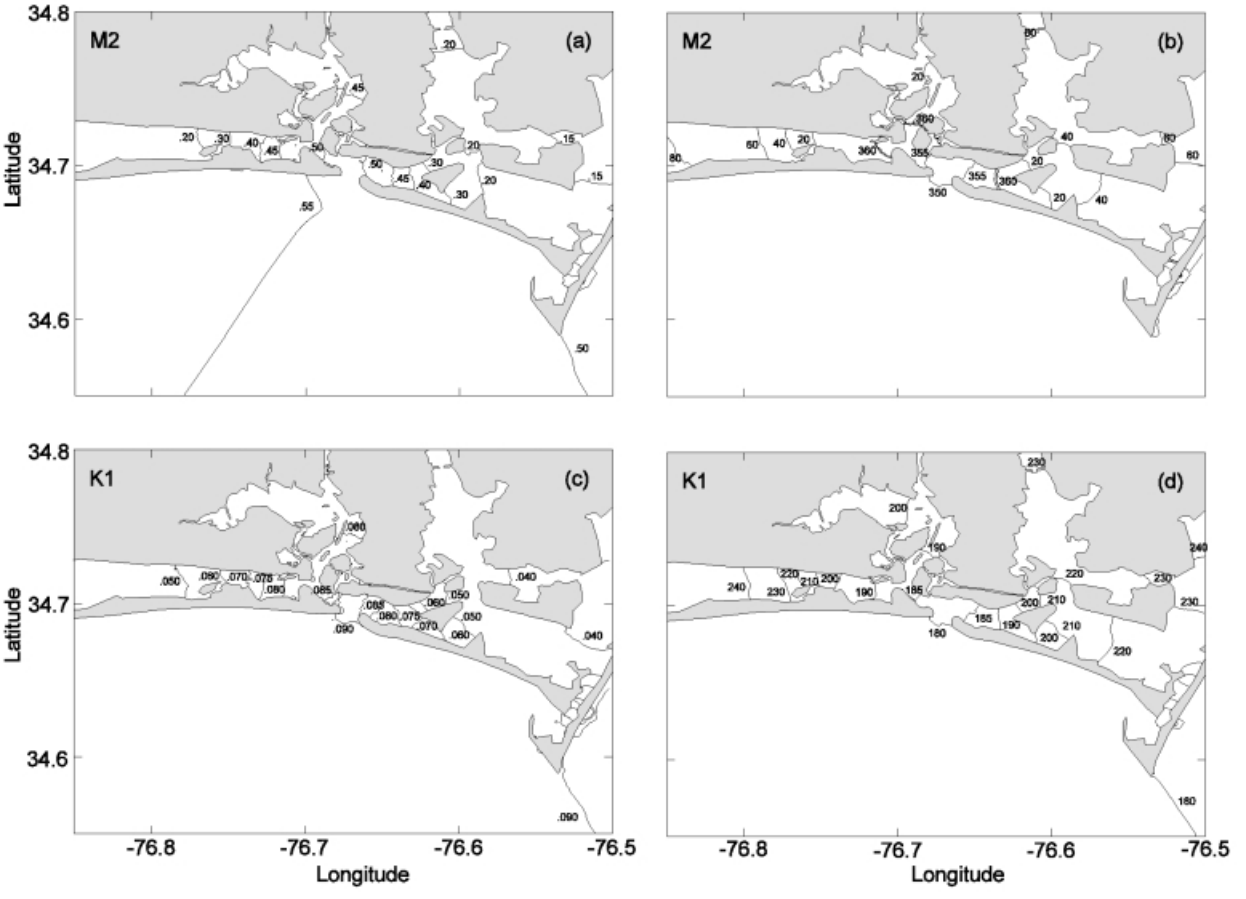

the inlet, and 'old' estuary water from the previous ebb plume that is re-entrained into the inlet along the western side. This corresponds closely to observations that, at the onset of flood tide, ocean water enters the estuary in roughly the eastern third of the inlet and is visually very distinct from water in the remainder of the inlet (R. Luettich, personal observation).

The vertically integrated Eulerian tidal residual velocity field generated by the model is shown in Fig. 6. This steady circulation, with maximum velocities of 15 cm s^{-1}, indicates the existence of offshore flow in the inlet channel and near-shore flow toward the inlet, as suggested by idealized barotropic inlet studies. However, the absence of counterrotating eddies on either side of the offshore flow represents a significant departure from these earlier studies. Instead, one large recirculation zone, approximately 4 km in diameter, appears to the west of this flow. At this point, we are pursuing additional studies to verify the existence of this feature and to identify factors (such as the angle of the inlet channel with respect to the coastline, the difference in the ebb tidal deltas on either side of the inlet) that may control its size and strength. The structure of the residual field suggests that a plume exiting the inlet would tend to move offshore, to the west, and might be re-entrained along the western side of the inlet, while offshore ocean water would be entrained along the eastern side. In the inlet throat, the residual flow is offshore on the western side of the inlet and onshore on the eastern side of the inlet. This is in good agreement with acoustic Doppler current profiler measurements made by Churchill *et al.* (1999) and current meter mooring data collected by Logan (1995). Inside the inlet, there appears to be a residual velocity directed from Shackleford Channel to Morehead Channel.

Model results were verified against water surface elevation and velocity data collected in the 1970s by the National Ocean Survey (Klavans, 1983). Observed tidal elevations at 16 stations in the vicinity of Beaufort Inlet (Fig. 7(a)) are compared with model results in Table 1. Both amplitude and phase are well simulated (typically within 10% amplitude and 10° phase) for the

Figure 5. Vertically integrated tidal velocities for the area around Beaufort Inlet: (a) slack before ebb; (b) maximum ebb; (c) slack before flood; (d) maximum flood.

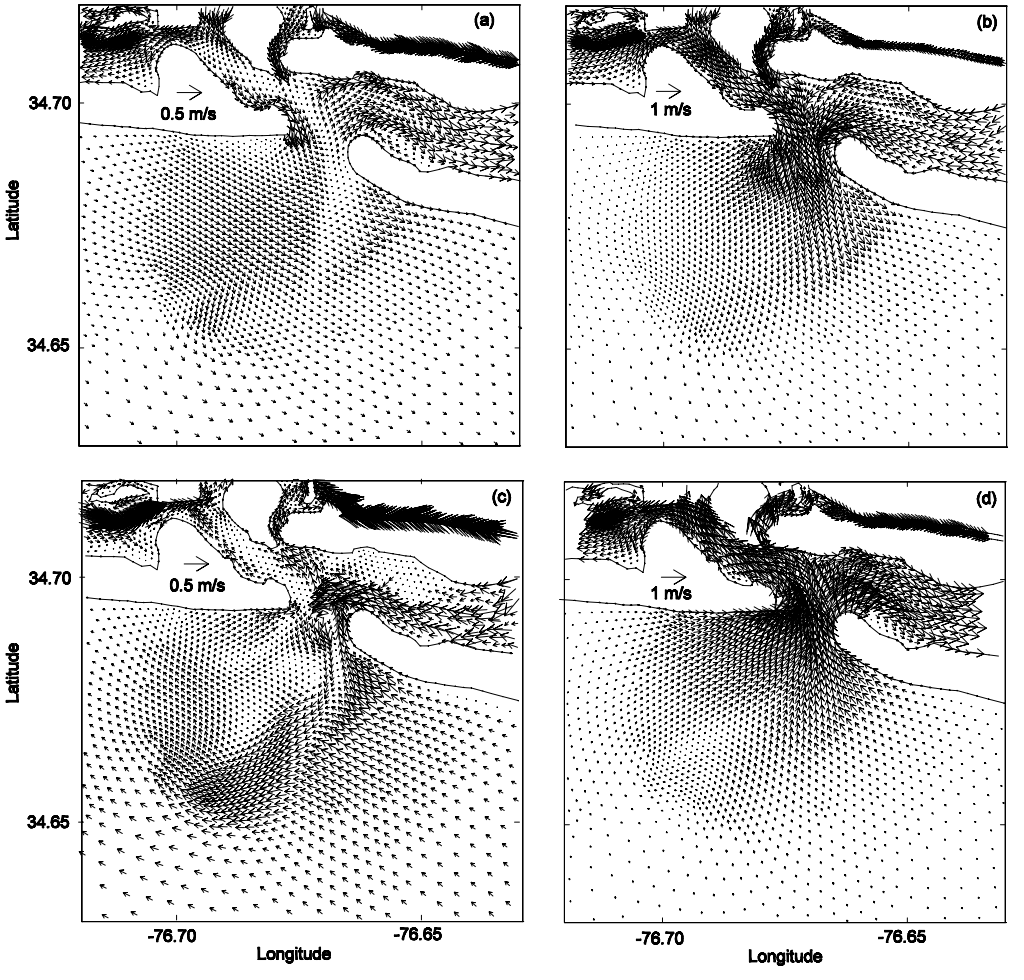

primary astronomical constituents. The M_2 phase is typically 10–20 min (5–10°) early in the model and this probably results from slight errors in the offshore boundary forcing. Other consistent differences between the model and the observational data occur at locations in small channels (such as stations 4 and 18) or furthest from the inlet (such as stations 5, 10 and 15). This is probably because of coarseness of the model grid (relative to some of the smaller bathymetric and geometric scales) and inaccurate bathymetry (which can shift significantly yet is rarely surveyed outside of the shipping channel). The M_4 overtide is not as well represented as the astronomical constituents; rather, this nonlinearly generated constituent is typically too large in the model. Generation of M_4 is strongly dependent on water depth (Grenier *et al.*, 1995) and geometric irregularities, suggesting that inaccurate bathymetry and shoreline representations account for a significant part of this problem. There is also some question about the fidelity of the observational data, since some closely spaced stations have very large differences in the observed M_4 component (such as stations 11 and 12).

Tidal velocity data are available for 10 positions near the inlet (Fig. 7(b)). Figure 8 presents comparisons between the modelled, depth-averaged tidal ellipses and observed tidal ellipses for the M_2 and K_1 tides. Flow is highly rectilinear and directed by the channel geometry. The model tends to underpredict the observed velocity magnitude in the inlet mouth (stations 6 and 7) by about 15% but reasonably reproduces the remaining velocity observations. Because of rapid bathymetric and geometric changes, flow near the inlet mouth is subject to strong horizontal shear. Therefore, these discrepancies may be the result of small spatial errors in current meter positions relative to the model

Figure 6. Vertically integrated, Eulerian tidal residual velocities near Beaufort Inlet.

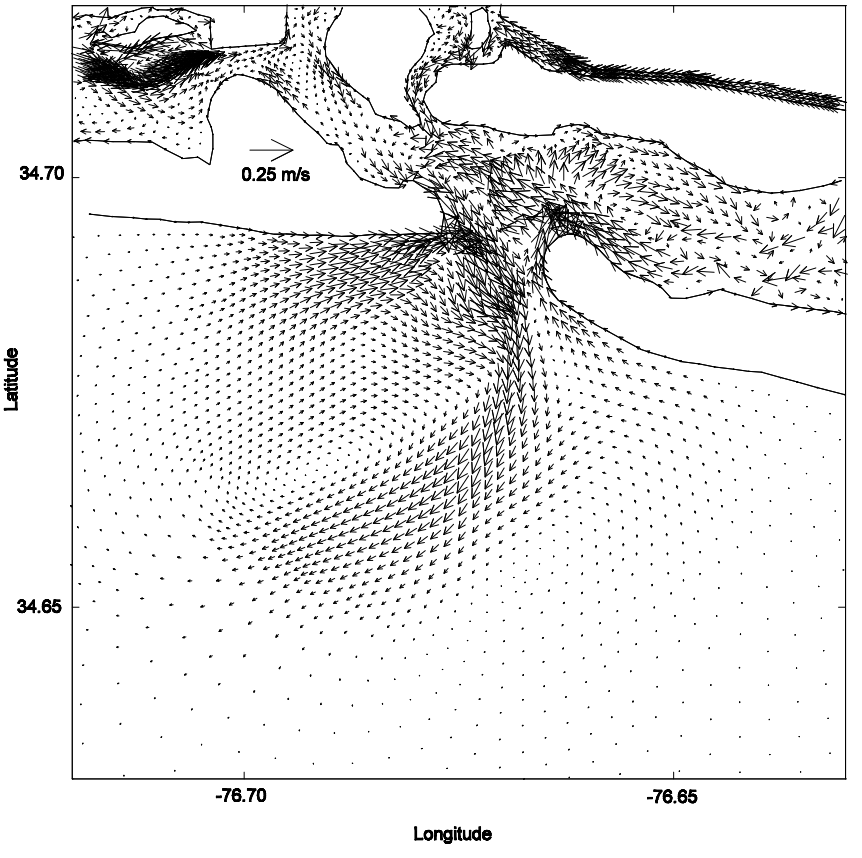

Figure 7. Locations of tidal elevation and velocity stations where observational data are available from a study by the National Ocean Survey (Klavans, 1983). Station numbering is from Klavans (1983).

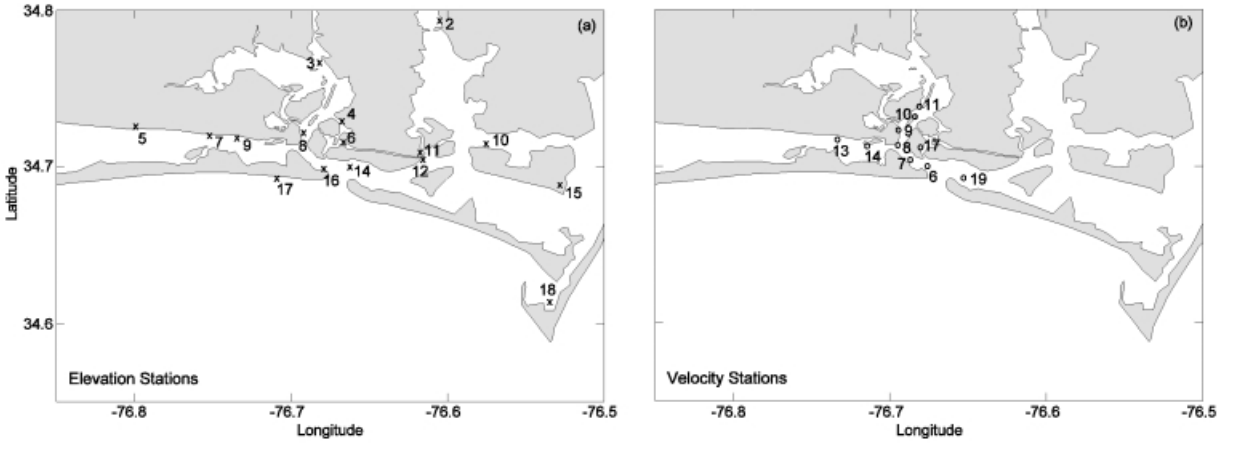

domain. The model has a sufficiently accurate representation of the channels in the vicinity of the inlet that the directions are well reproduced except at stations 9 and 11. These two stations are far up into the estuary, where model bathymetry or geometry presumably does not reflect local conditions.

Additional model verification was performed by comparing model fluxes through the three primary channels

Table 1. Comparison between modelled tidal elevation amplitudes and phases and NOS observational data (Klavans, 1983). Station numbering is from Klavans

	M_2				S_2				N_2			
	Elevation amplitude (m)		Phase (deg)		Elevation amplitude (m)		Phase (deg)		Elevation amplitude (m)		Phase (deg)	
Station	NOS	Model	NOS	Model	NOS	Model	NOS	Model	NOS	Model	NOS	Model
2	0.237	0.204	70	64	0.028	0.030	107	91	0.038	0.039	56	53
3	0.408	0.437	30	21	0.061	0.068	62	50	0.087	0.089	14	13
4	0.415	0.471	14	3	0.064	0.078	41	28	0.095	0.103	355	351
5	0.168	0.159	59	66	0.018	0.023	79	89	0.038	0.032	50	53
6	0.414	0.467	11	1	0.072	0.078	35	26	0.094	0.103	355	349
7	0.281	0.273	25	20	0.039	0.042	46	44	0.070	0.056	12	9
8	0.437	0.495	6	358	0.073	0.084	29	23	0.102	0.111	352	346
9	0.330	0.361	16	9	0.053	0.058	40	33	0.071	0.076	355	357
10	0.206	0.178	56	49	0.015	0.026	71	75	0.047	0.034	48	37
11	0.294	0.238	25	22	0.040	0.036	39	46	0.051	0.048	0	11
12	0.273	0.252	31	19	0.038	0.038	55	43	0.055	0.051	11	8
14	0.452	0.508	358	353	0.077	0.087	22	17	0.106	0.114	337	340
15	0.217	0.171	51	47	0.031	0.025	79	71	0.045	0.033	30	35
16	0.450	0.499	358	355	0.081	0.086	20	20	0.103	0.113	340	343
17	0.536	0.551	356	348	0.091	0.097	22	12	0.126	0.127	342	335
18	0.551	0.541	348	348	0.075	0.096	10	12	0.266	0.125	330	335
	O_1				K_1				M_4			
	Elevation amplitude (m)		Phase (deg)		Elevation amplitude (m)		Phase (deg)		Elevation amplitude (m)		Phase (deg)	
Station	NOS	Model	NOS	Model	NOS	Model	NOS	Model	NOS	Model	NOS	Model
2	0.044	0.039	244	242	0.048	0.044	239	232	0.026	0.032	79	76
3	0.059	0.061	216	210	0.071	0.077	210	199	0.021	0.043	4	352
4	0.061	0.064	208	202	0.076	0.082	203	190	0.001	0.012	60	246
5	0.040	0.044	273	251	0.044	0.049	223	241	0.006	0.008	12	13
6	0.056	0.063	208	202	0.076	0.082	201	188	0.004	0.016	270	223
7	0.049	0.052	245	225	0.054	0.060	206	212	0.010	0.019	334	275
8	0.064	0.064	204	200	0.077	0.084	196	187	0.006	0.015	308	192
9	0.055	0.058	215	213	0.064	0.070	208	200	0.013	0.021	289	267
10	0.037	0.037	265	234	0.045	0.042	221	224	0.004	0.015	85	51
11	0.054	0.046	217	217	0.078	0.053	199	206	0.015	0.017	212	342
12	0.049	0.046	223	217	0.060	0.054	219	205	0.001	0.010	357	343
14	0.063	0.065	199	196	0.080	0.087	192	183	0.001	0.021	275	191
15	0.043	0.036	232	232	0.051	0.041	229	222	0.018	0.017	19	30
16	0.061	0.064	200	198	0.091	0.085	186	185	0.008	0.024	252	188
17	0.067	0.070	194	191	0.097	0.093	199	179	0.008	0.025	169	198
18	0.084	0.070	208	191	0.079	0.093	178	178	0.007	0.022	279	195

NOS, National Ocean Survey.

inside the inlet with fluxes measured using a shipboard acoustic Doppler current profiler. These data were obtained from repeated passes across the channels during the second larval transport field experiment conducted in March 1996 (Churchill *et al.*, 1999). Model fluxes were computed by integrating the model results along lines matching the field tracks. The model underpredicts maximum flux through the small Radio Island Channel by as much as 50%, but is within about 15% of the observed flux through the main Morehead and Shackleford Channels (Fig. 9). In each channel, the model captures both the phasing and the diurnal inequality quite well.

Figure 8. Comparisons between modelled tidal ellipses (dotted) and observed tidal ellipses (solid) for M_2 and K_1 tidal constituents. Phases (degrees) are listed next to each ellipse.

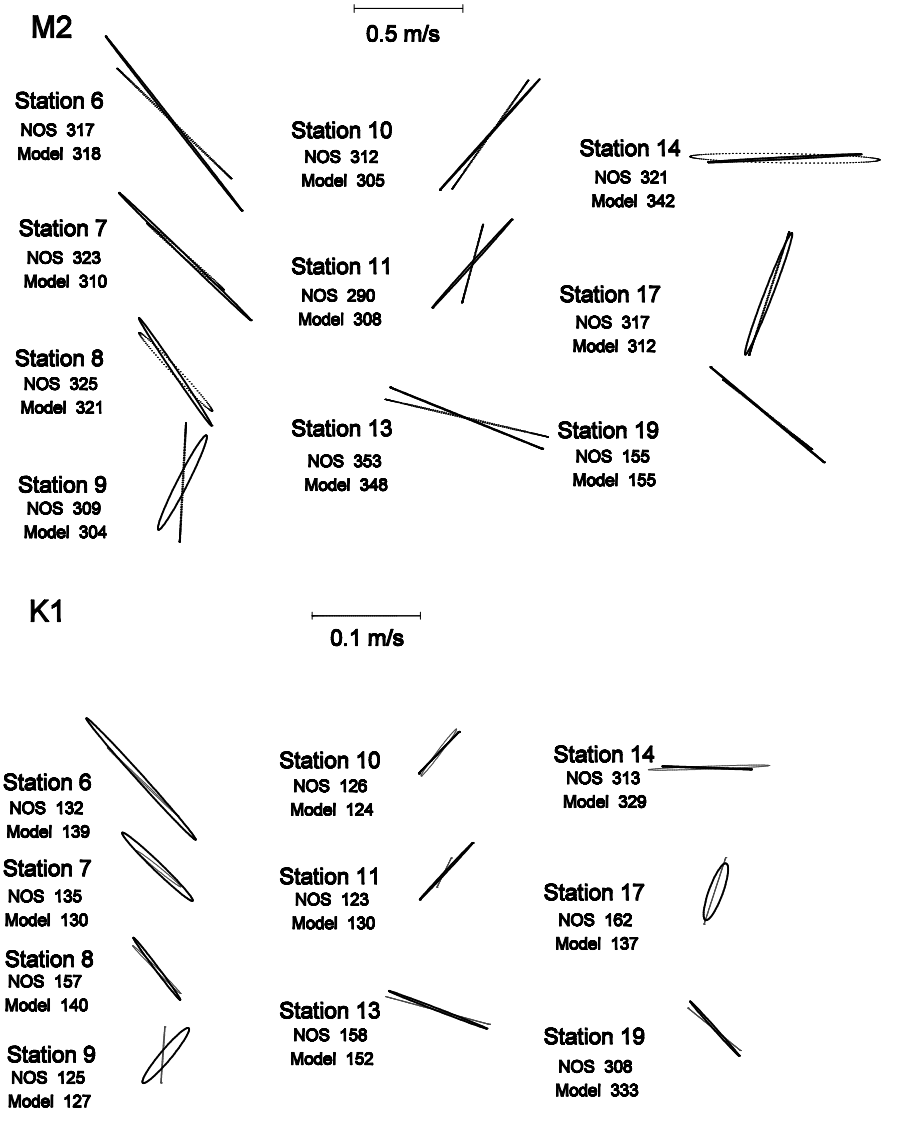

Wind model results

While tidal currents dominate the instantaneous flow near Beaufort Inlet and tidal dispersion can account for considerable net larval transport (see below), significant energy also exists at subtidal frequencies (Blanton *et al.*, 1999). In the presence of dominant tidal circulation, meteorologically forced subtidal circulation should be compared with the tidal residual circulation and with the tidal current shear, to determine the potential of the former to modify net transport as a result of tidal dispersion. We considered this effect by generating steady-state, three-dimensional circulation fields using the FUNDY5 model, driven by steady and spatially uniform wind fields that are climatologically representative of spring weather near Beaufort Inlet. Although wind events are clearly transient in nature, the shallow depths near the inlet suggest that the system will spin-up rapidly as it approaches steady state. Therefore, this limit is useful for an initial understanding of the role of wind in near-inlet circulation.

Since FUNDY5 is a linear model, it was necessary to develop a linear bottom friction coefficient and a constant-in-time vertical eddy viscosity that reflected turbulence generated via bottom mixing by the strong, tidally dominated currents. We computed a linear bottom friction coefficient k_l as

$$k_l = \frac{c_d|U|}{h} \tag{1}$$

where c_d is the quadratic drag coefficient (= 0.0025), h

Figure 9. Comparisons between tidal fluxes computed by the model with those measured using a shipboard acoustic Doppler current profiler during the March 1996 field experiments (Churchill *et al.*, 1999).

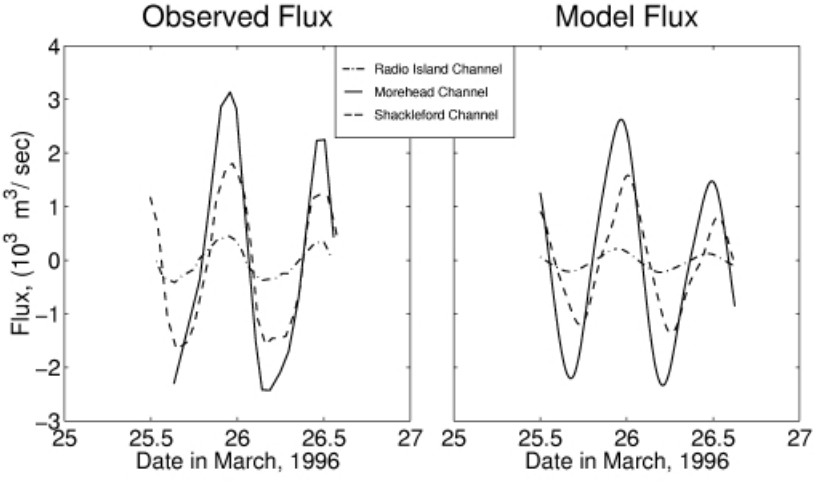

is the bathymetric depth and $|U|$ is a characteristic velocity magnitude. We computed the vertical eddy viscosity E_z as

$$E_z = 0.1hU* \quad (2)$$

where $U*$ is the friction velocity. Both $|U|$ and $U*$ were taken as spatially varying root mean square values determined from the ADCIRC solution. Minimum values were set, requiring $k_l > 0.000\ 025\ s^{-1}$ if $h > 50$ m and $E_z > 0.0005\ m^2\ s^{-1}$.

During the winter–spring period, the climatological mean wind speed as measured by an NOAA buoy near Cape Lookout, NC, is approximately 6 m s^{-1} with a standard deviation of 2.5 m s^{-1}. The direction toward which the wind blows ranges from north-east to south-east, with an average direction being toward the east during March (Werner *et al.*, 1999). We illustrate basic characteristics of the wind-driven circulation near Beaufort Inlet by presenting the modelled current field at the surface and at the lowest grid point (essentially 1 m above the bottom) for a wind of 7.5 m s^{-1} directed toward the east (Figs 10(a) and 10(b)) and directed toward the north (Figs 10(c) and 10(d)).

Because of the shallow water depths, the surface Ekman layer is depth-limited and eastward wind generates eastward-flowing surface currents with velocities of order 10 cm s^{-1} outside the inlet (Fig. 10(a)). The orientation of Beaufort Inlet is such that part of this eastward flow is directed into the inlet and is then driven eastward behind Shackleford Banks, through Core Sound and ultimately into Pamlico Sound. Because the eastward wind is roughly parallel to the shoreline in this area, there are few locations where water may pile up against the shore and generate reversing flows at depth. Therefore, near-bottom currents (Fig. 10(b)) closely resemble surface currents, except that they are diminished in magnitude, because of frictional effects.

The wind blowing toward the north generates weaker surface currents (less than 5 cm s^{-1}) that are aligned with the wind, so are directed primarily onshore (Fig. 10(c)). Water is driven directly into the inlet and then up estuary through the Morehead, Radio Island and Shackleford Channels. Away from the inlet mouth, water piles up along Shackleford Banks and Bogue Banks, driving an offshore flow at depth. However, near the inlet mouth and inside the inlet, the flow is primarily unidirectional over the depth.

Since the FUNDY5 model is linear, its response to winds of different speed and direction follows directly from these examples. A different strength wind will drive proportionally stronger or weaker currents. (Since the surface stress is quadratic in wind speed, this will occur in proportion to the square of the wind speed.) A wind that blows toward any direction other than north or east will generate a circulation that is the vector sum of that driven by the northward component of the wind and that driven by the eastward component of the wind.

Although the wind-driven residual currents are generally weaker than are the tidal residual currents, the wind-driven currents appear strong enough and appear to have areas of sufficient lateral shear to affect larval transport and dispersion in the vicinity of the inlet, particularly under strong wind conditions.

Figure 10. Steady state circulation near Beaufort Inlet driven by a wind of 7.5 m s^{-1}: (a) surface currents as a result of a wind blowing towards the east; (b) near-bottom currents (1 m above bottom) as a result of wind blowing towards the east; (c) surface currents as a result of wind blowing towards the north; (d) near-bottom currents (1 m above bottom) as a result of wind blowing towards the north.

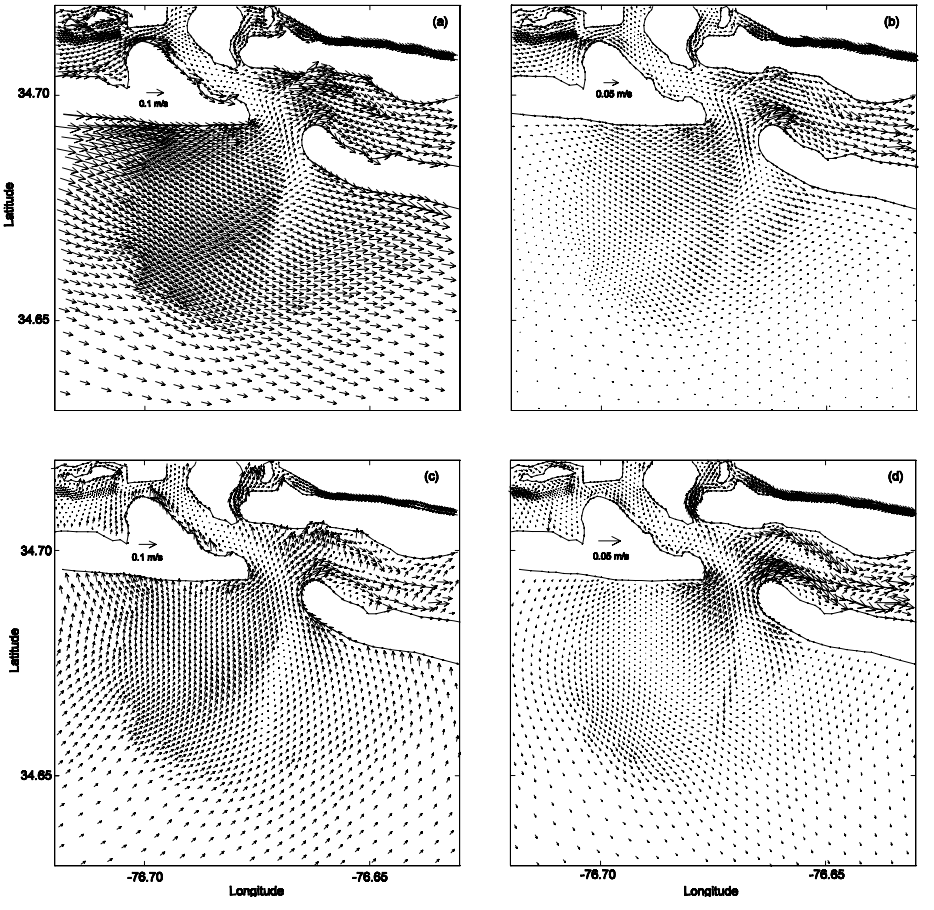

SIMULATED LARVAL TRANSPORT

Flow fields from the tidal and wind-driven models were used as input to a particle-tracking model (Baptista *et al.*, 1984; Foreman *et al.*, 1992) to examine potential larval transport pathways in the vicinity of Beaufort Inlet. The particle-tracking model was initiated with a rectangular array of 200 particles in one of three locations (west, centre or east) outside the inlet (Fig. 11). Each particle-tracking model run had a duration of 10 M_2 tidal cycles (about 124 h), which is a typical time period over which larvae in this stage might remain in the water column (R. Forward, pers. comm.). As described in detail in the following, a large number of particle-tracking model runs were conducted to determine passive transport under mean tidal conditions, the spring-neap cycle, and wind-plus tidally forced conditions.

Results are presented quantitatively in terms of the number of particles crossing 'virtual nets' that were placed across the channels immediately inside Beaufort Inlet at the approximate positions of plankton-sampling stations during the March 1996 field experiment (Fig. 11). Net-crossing statistics of model runs with 2000 particles were found to be nearly identical to those from runs with 200 particles, so the smaller number of particles was used for all runs presented in the following. We note that larval sampling conducted during the field study used nets that were relatively small compared with the channel width, so capturing only a tiny fraction of the total fish that passed any location. In trying to represent this with the model and at the same time keeping the particles to a computationally manageable number, we have used nets spanning the entire channel and allowed the particles

Figure 11. West, centre and east initial positions for the 200 particles used in particle model runs. Heavy lines show the positions of 'virtual nets' used to quantify the number of particles passing through the Morehead, Radio Island and Shackleford Channels.

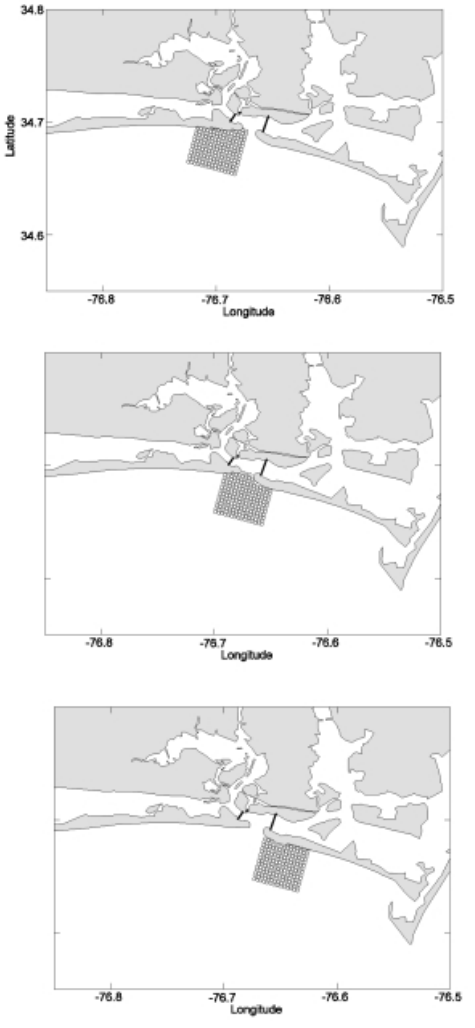

to remain in the water column after crossing a net. However, to eliminate the effect of single particles being trapped near a net and crossing it multiple times, particles were only counted the first time that they crossed each net.

Mean tidal forcing

The principal tidal forcing in this region is the semidiurnal M_2 constituent. Therefore, we initially simulated larval transport associated with this constituent plus its principal nonlinear overtide (M_4) plus the nonlinearly generated tidal residual circulation. The trajectories (after 10 M_2 tidal cycles) of all the particles,

Figure 12. 10-day trajectories for particles released at slack before ebb and transported by M_2 + M_4 + steady residual tidal currents.

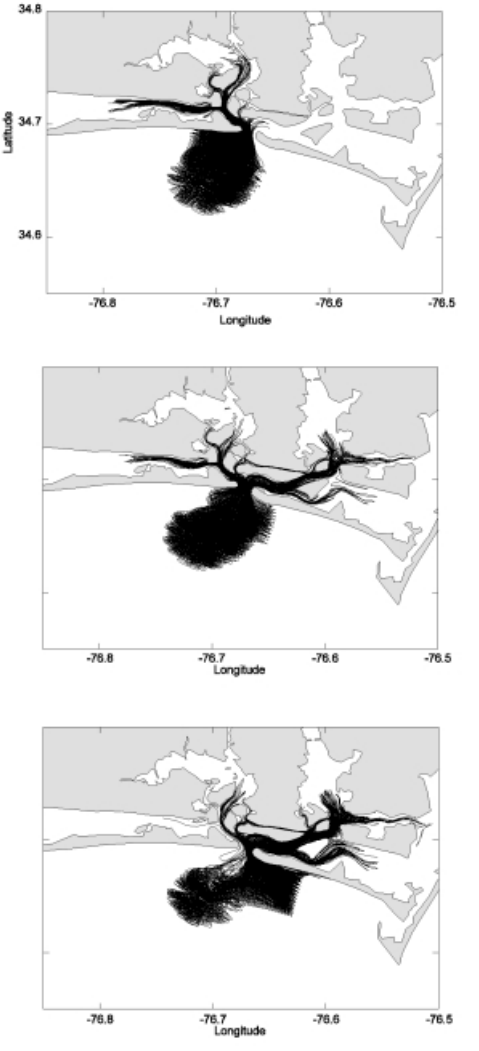

assuming a slack before ebb release time, are shown in Fig. 12. Particles released west of the inlet are almost exclusively transported up Morehead Channel into the Newport River Estuary and Bogue Sound. Particles released in the centre of the inlet are transported through Morehead Channel, Radio Island Channel and Shackleford Channel. Particles released east of the inlet are primarily transported into Shackleford Channel, although a significant fraction is transported into Radio Island and Morehead Channels. Also, these trajectory lines show a tendency for particles to become entrained in the residual eddy located outside and west of the inlet (Fig. 6).

Although Fig. 12 shows that the trajectory of a particle is dependent on its release point in space, the trajectory also depends on a particle's release time

during the tidal cycle. Therefore, for each of the three spatial initial conditions, 10 model runs were conducted with starting times that were evenly incremented through the tidal cycle. The average number of net crossings as well as the standard deviation were computed for each ensemble of 10 model runs and are reported in Table 2. The average number of net crossings confirms the patterns depicted in Fig. 12. Over half the particles released west of the inlet progress up Morehead Channel, while only a few pass through Radio Island Channel and virtually none moves through Shackleford Channel. Centre release results in nearly equal numbers of particles passing through Morehead and Shackleford Channels. East release results in three-quarters of the particles passing through Shackleford Channel, and approximately 10% passing through Radio Island and Morehead Channels. These results also show that about half the particles did not cross any nets for west and centre releases, although only about a quarter of the particles did not cross a net for the east release. The standard deviations are typically small compared with the means, indicating that there is some sensitivity of the particle track to starting time during the tidal cycle, but that the overall patterns are relatively independent of starting time.

Animations of particle trajectories (not shown) indicate that the principal pathways that particles follow into the inlet are via the near-shore regions where the tidal residual circulation is strong and directed toward the inlet.

Spring-neap effects

The influence of the spring-neap cycle was considered by repeating the runs described already but including the S_2 tidal constituent which, in combination with the M_2 constituent, generates the spring-neap cycle. In this case, two sets of runs were conducted: one in which the run period was centred around the neap tide and one in which the run period was centred around the spring tide. Statistics for particles not crossing any nets suggest that transport into the estuary during spring (neap) tide increases (decreases) by about 15–20% compared with the M_2 tide alone (Table 2). Net-crossing statistics suggest that most of the increase (decrease) in particles entering the estuary occurs in the channel closest to the release points. For example, for a west release, the number of particles entering Morehead Channel increases (decreases) on the spring (neap) tide. The spring tide also appears to be more effective at transporting particles from west to east across the inlet (such as particles passing the Shackleford net that were initially released west of the inlet) than is either the neap or the mean tide. In fact, during the spring tide, exchange between the Morehead and Shackleford Channels is approximately equal in both the east and west directions, whereas west-to-east exchange is essentially nil for the other conditions. Enhanced transport through Shackleford Channel following a west release appears to occur at the expense of transport through Radio Island Channel, suggesting that, on spring tide, particles may overshoot Radio Island Channel and move through Shackleford Channel instead.

Combined wind and tide effects

Subtidal wind-driven circulation combines with tidal residual currents to alter the characteristics of inlet exchange. To investigate this effect, wind-driven FUNDY5 model results were added to the tidal residuals to generate a combined residual current that was used with the mean tidal currents (M_2 + M_4) in an

Table 2. Net-crossing statistics for particle -tracking model runs with tides only

Release location	Morehead Channel		Radio Island Channel		Shackleford Channel		Did not enter	
	Mean (%)	Stand. dev. (%)	Mean (%)	Stand. dev. (%)	Mean (%)	Stand. dev. (%)	Mean (%)	Stand. dev. (%)
M_2 + M_4 + residual								
West	55	9	4	2	1	1	44	8
Centre	30	7	7	3	31	9	44	6
East	12	1	8	1	74	3	26	3
S_2 + M_2 + M_4 + residual at neap tide								
West	48	8	8	3	1	1	52	8
Centre	28	7	7	2	26	8	51	8
East	15	2	7	2	69	2	31	2
S_2 + M_2 + M_4 + residual at spring tide								
West	63	6	1	1	10	3	34	4
Centre	33	8	7	3	44	10	33	5
East	11	2	14	2	79	4	21	4

Stand. dev., standard deviation.

additional series of particle-tracking model runs. To account for vertical structure in the wind-driven currents, separate runs were made for particles released at the surface, mid-depth and near bottom (i.e. at the lowest grid point in the FUNDY5 model). Although larvae may be vertically mixed by turbulence while transiting the inlet, no attempt was made to mix particles vertically during the course of particle tracking. Instead, the surface and bottom runs were considered to represent limiting cases for larvae that are able actively to regulate their position in the water column, while the mid-depth run was assumed to be at least partially representative of larvae mixed through the water column.

To account for the range of possible wind conditions, wind speeds of 5 and 10 m s^{-1} blowing in eight evenly spaced coordinate directions (i.e. N, NE, E, SE, S, SW, W, NW) were considered. As before, the results represent an ensemble of net crossings from particles released at 10 evenly spaced times during the M_2 tidal cycle that are transported passively for 10 M_2 tidal cycles. We note that wind events are rarely constant for

Figure 13. Net-crossing statistics for 10 M_2 tidal cycle long particle-tracking runs using combined wind-driven and mean tidal currents. Each graph shows the average percentage of particles released west of the inlet, at the specified depth, at 10 evenly spaced phases of the tide that either crossed the listed net or crossed none of the nets. The dotted circle in each graph represents net crossings under the mean tidal conditions with no wind. For Radio Island Channel, full scale is 40% of the initially released particles, while full scale is 100% for the other graphs.

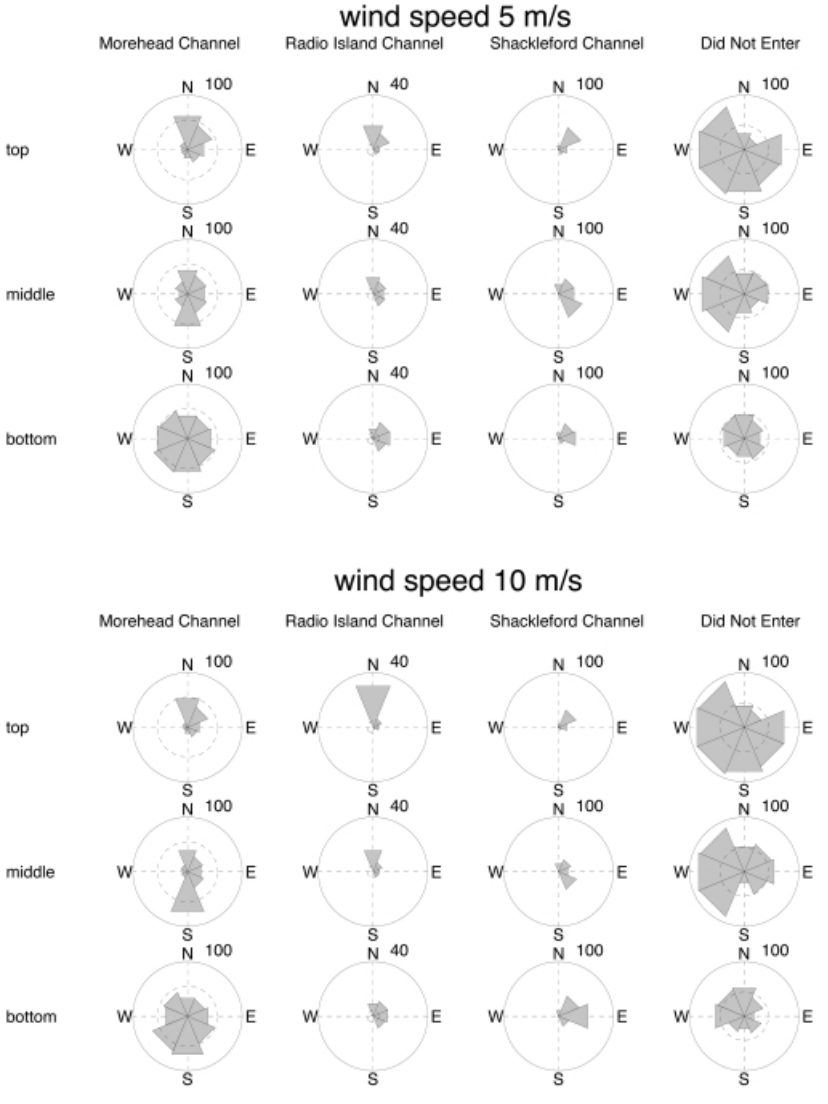

Figure 14. Net-crossing statistics for 10 M_2 tidal cycle long particle-tracking runs using combined wind-driven and mean tidal currents. Each graph shows the average percentage of particles released across the centre of the inlet, at the specified depth, at 10 evenly spaced phases of the tide that either crossed the listed net or crossed none of the nets. The dotted circle in each graph represents net crossings under the mean tidal conditions with no wind. For Radio Island Channel, full scale is 40% of the initially released particles, while full scale is 100% for the other graphs.

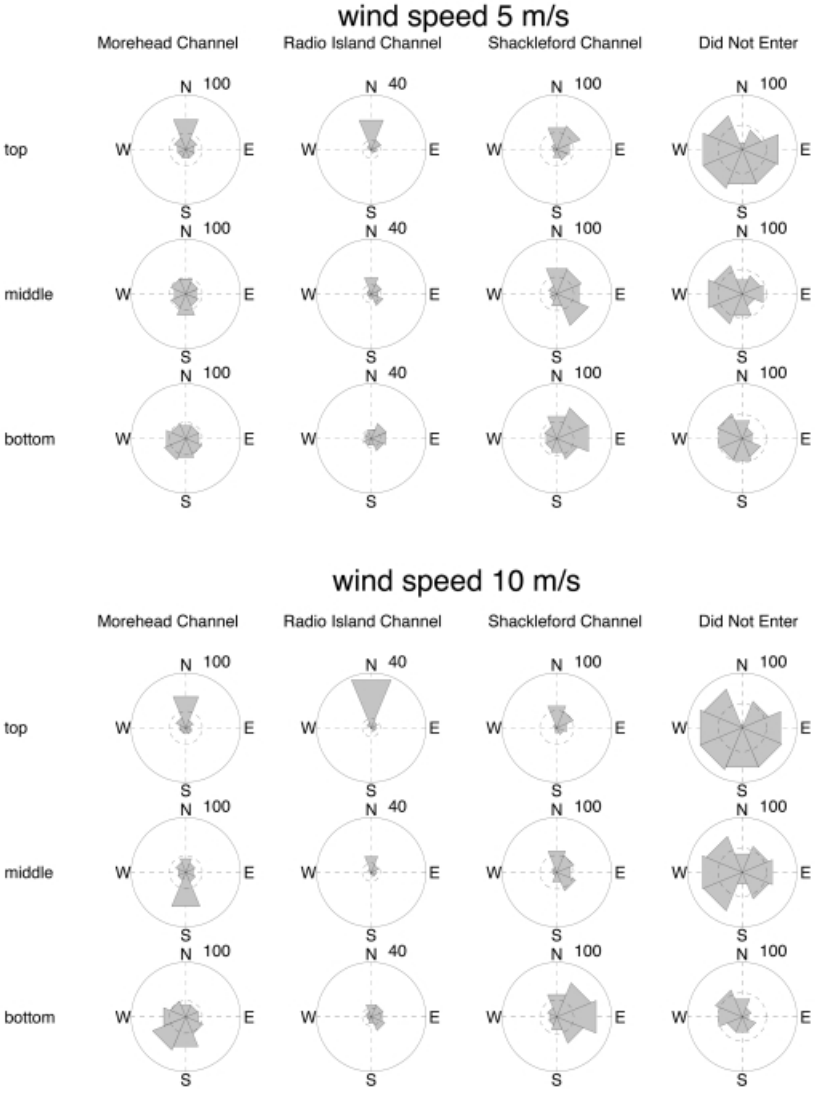

five days in this region, so results from this section are probably overestimates of the true impact of wind on larvae ingress.

Figures 13–15 show results for particles released west, across the centre and east of the inlet respectively. The figures represent the percentages of initial particles that crossed a specified net as a function of the direction toward which the wind was blowing. A dotted circle is superimposed on each graph to represent the percentage net crossings in the absence of wind (i.e. as specified in the upper section of Table 2).

Particles released west of the inlet

Winds blowing toward the north or north-east enhance total inlet ingress at the surface (shown by a drop in the number of surface particles that did not enter as compared with the case of tides only; Fig. 13) by propelling particles into a favourable position for transport by the flood tide. Wind-driven currents accomplish this by moving particles broadly closer to the inlet or into the near-shore zone, where the net transport is driven by the strong inlet-directed tidal residual currents found there (Fig. 6). Winds in all

Figure 15. Net-crossing statistics for 10 M_2 tidal cycle long particle-tracking runs using combined wind-driven and mean tidal currents. Each graph shows the average percentage of particles released east of the inlet, at the specified depth, at 10 evenly spaced phases of the tide that either crossed the listed net or crossed none of the nets. The dotted circle in each graph represents net crossings under the mean tidal conditions with no wind. For Radio Island Channel, full scale is 40% of the initially released particles, while full scale is 100% for the other graphs.

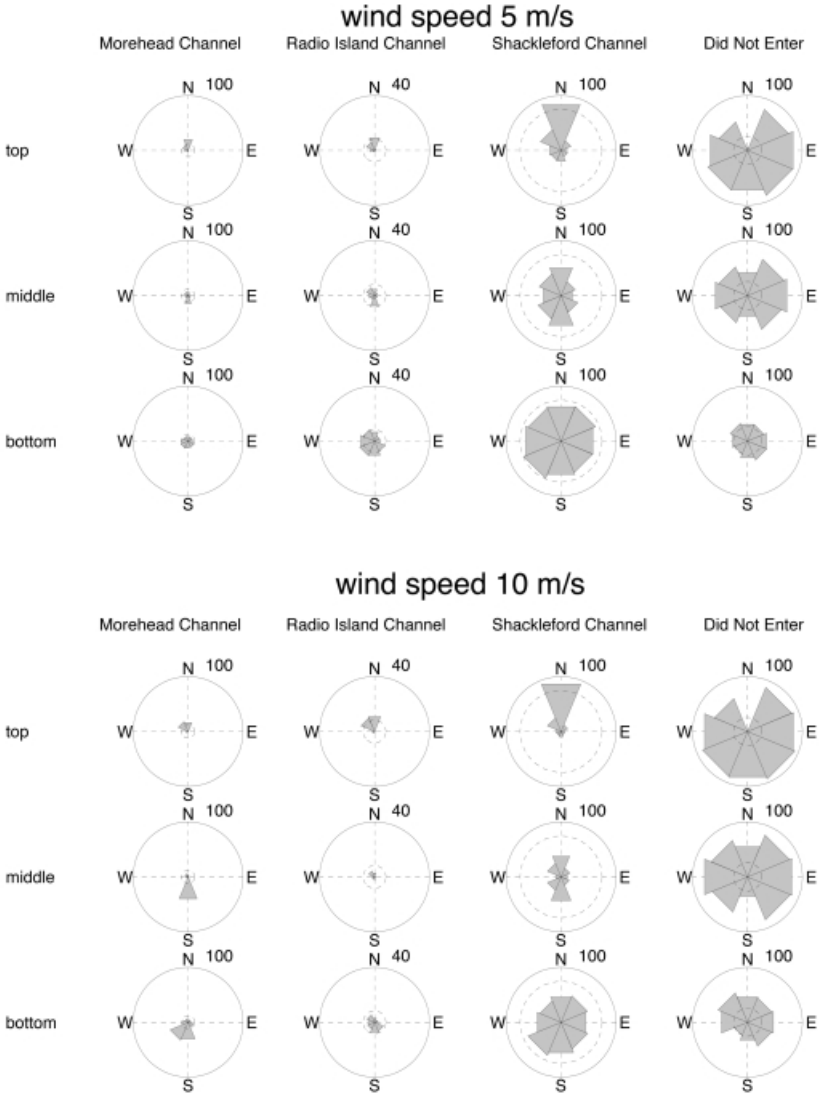

other directions either blow surface particles away from the inlet or offshore, so decrease ingress. Bottom ingress is enhanced by winds with eastward and southward components. Southward winds transport bottom particles in the onshore direction, while eastward winds transport bottom particles toward the inlet. At mid-depth, enhanced ingress also occurs primarily as a result of southward winds although this enhancement was significant only for the 10 m s^{-1} wind speed.

Winds generally reduce particle ingress through Morehead Channel. Southward winds are the exception, because the slight increase in total ingress at the bottom appears to be transported up estuary through Morehead Channel. For northward winds, increased total ingress through the inlet plus some of the purely tidal ingress in Morehead Channel are diverted to Radio Island Channel. This appears to be as a result of the up-estuary residual circulation close to the mouth and along the length of Radio Island Channel generated by a north wind (Figs 10(c) and 10(d)). This effect is strong enough that, for the wind speed of 10 m s^{-1}, the number of particles moving through Radio Island

Channel is comparable with that through the much larger Morehead Channel. Eastward winds generate up-estuary currents in Radio Island Channel and Shackleford Channels, so enhancing particle transport through both. Enhanced surface transport into the inlet that occurs with north-eastward wind moves primarily up Shackleford Channel. Eastward and south-eastward winds decrease total ingress at the surface, by blowing particles out of the inlet. However, these wind-driven currents are weaker at the bottom, so are less able to move particles away from the inlet. Instead, it seems that particles are pushed to the east side of the inlet, where they progress up Shackleford Channel. Ingress through Shackleford Channel increases from essentially nil for purely tidal currents to slightly larger than that through Morehead Channel for a wind speed of 10 m s^{-1}.

Particles released across the centre of the inlet

Wind blowing towards the north is particularly effective at enhancing ingress of surface particles as 88% and 94% crossed at least one of the nets for the wind speeds of 5 and 10 m s^{-1} respectively (compared with only 56% for the purely tidal circulation). The northward wind keeps particles close enough to the inlet such that they can be advected in on a flood tide. Winds blowing in other directions decreased ingress, by creating a surface residual current either offshore or away from the inlet on the downwind side. At the bottom, northward winds also tend to enhance ingress, by driving a current toward the inlet in the inlet centre (Fig. 10(d)). However, a southward wind also enhances ingress, by driving an onshore bottom current both on the eastern and the western sides of the inlet, which brings particles into the near-shore zone where they can then be transported into the inlet by the tidal residual circulation. In addition, an eastward wind enhances bottom ingress, since it generates currents into the inlet that are not strong enough to push particles past the inlet to the east as occurs at the surface. Particles at mid-depth reflect both the surface and bottom behaviours to varying degrees, as ingress is enhanced by both northward and southward winds.

Particles entering at the surface with a northward wind move up estuary through all three inner channels. As before, the largest proportional increase compared with the purely tidal case occurs in Radio Island Channel. Particles entering at the bottom with a southward wind primarily move up Morehead Channel, since this wind generates down-estuary currents in both Radio Island and Shackleford Channels. Particles entering at the bottom with an eastward wind favour up-estuary transport mainly via Shackleford Channel. With this wind, particle numbers are several times greater in Shackleford Channel than is the case in Morehead Channel, as compared with being nearly equally distributed between these channels with purely tidal circulation.

Particles released east of the inlet

Consistent with the other release locations, winds blowing northward are extremely efficient at enhancing surface drifter ingress, as 95% and 97% of the particles crossed at least one of the nets for the wind speeds of 5 and 10 m s^{-1} respectively. Interestingly, no other wind direction enhances larvae ingress at any level in the water column. This is partly because of a relatively high percentage of particles entering the inlet under purely tidal conditions (Table 2). Particle loss from the inlet system was much greater at the surface than it was at depth, presumably because of correspondingly higher wind-driven current speeds. Surface ingress into all three channels was enhanced by the northward wind, while north-westward and southward winds redirect particles from Shackleford Channel into Morehead Channel.

DISCUSSION AND CONCLUSIONS

This study considers barotropic circulation and transport in the vicinity of Beaufort Inlet, NC. Observations indicate that this inlet is weakly stratified at most times (see, for example, Blanton *et al.*, 1999; Churchill *et al.*, 1999), making the barotropic case an important part of a complete understanding of the circulation at this and similar barrier island inlets. We have developed a highly accurate model representation of the inlet geometry and tidal circulation, but simplified the problem by considering steady-state wind responses and restricting particles to remaining passively at the top, middle or bottom of the water column throughout their transit.

Given the high number of scenarios investigated, the assumption of a steady-state wind response was a practical necessity and should not be too unreasonable, owing to the shallow water depths and, hence, rapid spin-up time of the system. However, since weather systems are not normally stationary in this area for as long as 10 M_2 tidal cycles (the duration of the particle-tracking model runs), the computed wind effects on larval transport are probably overestimates of what might actually be expected. Nevertheless, the results provide useful insight into characteristic behaviours of the system for various wind conditions.

An earlier study (Luettich *et al.*, 1998) has shown that simple day–night vertical migratory behaviour causes minimal departure from passive particle transport patterns during March (the primary migratory period in

the inlet part of the SABRE programme), because the day–night cycle and the tidal cycle have nearly the same duration at this time of year. Larvae that move to the bottom at daybreak to avoid visual predation, such that they cease to be transported horizontally, move back up into the water column the following nightfall at approximately the same phase of the tide during which they left. As a result, they follow horizontal paths that are nearly equivalent to those of purely passive particles. Larval catches during the March 1996 field experiments at Beaufort Inlet showed that, in the channels inside the inlet, larvae appeared to be undergoing selective tidal stream transport in which they were mostly present in the water column during nighttime flood tides (Churchill *et al.*, 1999; Forward *et al.*, 1999). However, larval catches in the inlet mouth are not as conclusive and, in general, it is not known where in the system larvae begin this behaviour. By considering passive particle transport, we are only assessing larval transport potential. However, this is a necessary and important step toward understanding more complex larval transport, particularly given the unknowns in larval behaviour outside the inlet.

The vertically integrated ADCIRC tidal model, yielded good agreement with National Ocean Survey tidal data and observations collected during the March 1996 field study. The nonlinearly generated residual current patterns are consistent with available field data and idealized barotropic inlet studies that show offshore-directed flow in the middle of an inlet and flow toward the inlet in the near-shore zones on either side. However, in contrast to an idealized barotropic tidal inlet, the model indicates that a significant residual eddy exists only west of the offshore flow. The structure of the current field suggests that water exiting the inlet would preferentially move offshore, to the west and be re-entrained along the western side of the inlet, while offshore ocean water would be most readily entrained along the eastern side of the inlet. Wind-driven currents generated with the three-dimensional FUNDY5 model are generally weaker than are the tidal residual currents, although they appear significant enough to affect larval transport in the vicinity of the inlet, particularly during strong wind conditions.

Particle-tracking model runs indicate that, under mean tidal forcing, particles initially released west of the inlet enter the inlet and are transported up-estuary via Morehead Channel. Virtually none crosses the inlet from west to east to move through Shackleford Channel. Particles released across the inlet mouth enter the inlet and are transported up estuary in roughly equal proportions through Morehead and Shackleford Channels. A significantly higher percentage of particles released east of the inlet actually ingress into the system when compared with those released west of and across the inlet mouth. The up-estuary transport of these particles is primarily through Shackleford Channel, although 10–20% of the particles are able to cross the inlet from east to west, so enter through Morehead Channel. Ingress occurs primarily in the near-shore zone that is characterized by tidal residual currents directed toward the inlet. Spring (neap) tide increases (decreases) net particle ingress by 15–20% over the mean tide conditions. During spring tide, exchange between Morehead and Shackleford Channels is approximately equal in both east and west directions.

Particle-tracking model runs that include both wind-driven and the mean tidal circulation indicate that only a narrow range of wind directions significantly enhances particle ingress (compared with ingress as a result of the mean tide alone), while a wide range of wind conditions significantly decrease particle ingress. Northward wind most effectively increases ingress of surface particles from all areas outside the inlet, by pushing these particles either directly into the inlet or into the near-shore zone where tidal currents are favourable for ingress. Inside the inlet, the particle transport path that experiences the greatest increase on a northward wind is Radio Island Channel. This occurs because a northward wind generates an up-estuary circulation near the mouth of Radio Island Channel and along its length. No other wind enhances particle ingress at the surface, mid-depth or bottom from the east side of the inlet. At the bottom of the water column, ingress is enhanced from the centre and the west side of the inlet by southward and eastward winds. Southward wind drives an onshore flow at depth on either side of the inlet, which transports particles onshore and, hence, into the ingress-favourable near-shore zone. An eastward wind moves particles at depth toward the eastern side of the inlet, where they are efficiently transported into the inlet by the tidal circulation. Inside the inlet, particle transport is enhanced in Morehead Channel by southward wind and in Shackleford Channel by eastward wind. Particles at mid-depth reflect both surface and bottom behaviours to varying degrees. In general, their movement is closer to bottom particles for a wind speed of 5 m s^{-1} and closer to surface particles for a wind speed of 10 m s^{-1}. Stronger wind deepens the surface layer and, therefore, directly influences more of the water column than does lighter wind.

Returning to the observation that nearly an order of magnitude more larvae were collected in Shackleford Channel than in Morehead Channel during the larval transport field experiments in March 1996, our modelling

indicates that, in the absence of wind effects, these larvae must have approached Beaufort Inlet primarily from the east to have attained such a distribution inside the inlet. If the larvae approached Beaufort Inlet in a relatively uniform spatial distribution that spanned both sides of the opening, then the only mechanism for concentrating their numbers in Shackleford Channel vs. Morehead Channel would be an eastward wind. While the climatological mean wind direction in this region is eastward during March, there were no significant eastward winds observed during the March 1996 experiments.

REFERENCES

Baptista, A.M., Adams, E.E. and Stolzenbach, K.D. (1984) Eulerian–Lagrangian analysis of pollutant transport in shallow water. *MIT RM Parsons Lab. Tech. Rep. No. 296*. Massachusetts Institute of Technology, Cambridge, MA.

Blanton, J.O., Amft, J., Luettich, R.A. Jr, Hench, J.L. and Churchill, J.H. (1999) Tidal and subtidal fluctuations in temperature, salinity and pressure for the winter 1996 larval ingress experiment—Beaufort Inlet, NC. *Fish. Oceanogr.* **8**(Suppl. 2):134–152.

Chao, S.-Y. (1990) Tidal modulation of estuarine plumes. *J. Phys. Oceanogr.* **20:**1115–1123.

Chen, Y.-H., Shaw, P.-T. and Wolcott, T.G. (1997) Enhancing estuarine retention of planktonic larvae by tidal currents. *Estuar. Coast. Shelf Sci.* **45:**525–533.

Churchill, J.H., Forward, R.B., Luettich, R.A. Jr, Hench, J.L. Hettler, W.F., Crowder, L.B. and Blanton, J.O. (1999) Circulation and larval fish transport within a tidally dominated estuary. *Fish. Oceanogr.* **8**(Suppl. 2):173–189.

DeVries, M.C., Tankersley, R.A., Forward, R.B. Jr, Kirby-Smith, W.W. and Luettich, R.A. Jr (1994) Abundance of estuarine crab larvae is associated with tidal hydrologicvariables. *Mar. Biol.* **118:**403–413.

Fore, P.L. and Baxter, K.N. (1972) Diel fluctuations in the catch of larval gulf menhaden, *Brevoortia patronus*, at Galveston entrance, Texas. *Trans. Am. Fish. Soc.* **101:**729–732.

Foreman, M.G.G., Baptista, A.M. and Walters, R.A. (1992) Tidal model studies of particle trajectories around a shallow coastal bank. *Atmos.-Ocean* **30:**43–69.

Forward, R.B. Jr, Reinsel, K.A., Peters, D., Tankersley, R.A., Churchill, J.H., Crowder, L., Hettler, W.F., Warlen, S.M. and Green, M. (1999) Transport of fish larvae through a tidal inlet. *Fish. Oceanogr.* **8**(Suppl. 2):153–172.

Geyer, W.R. and Signell, R.P. (1992) A reassessment of the role of tidal dispersion in estuaries and bays. *Estuaries*. **15:**97–108.

Grenier, R.R. Jr, Luettich, R.A. Jr and Westerink, J.J. (1995) A comparison of the frictional characteristics of two-dimensional and three-dimensional tidal models. *J. Geophys. Res.* **100C:**13719–13735.

Hill, A.E. (1991) A mechanism for horizontal zooplankton transport by vertical migration in tidal currents. *Mar. Biol.* **111:**485–492.

Kapolnai, A., Werner, F.E. and Blanton, J.O. (1996) Circulation, mixing and exchange processes in the vicinity of tidal inlets: a numerical study. *J. Geophys. Res.* **101**(C6)**:**14253–14268.

Klavans, A.S. (1983) Tidal hydrodynamics and sediment transport in Beaufort Inlet, North Carolina. *NOAA Tech. Rep. No. 100*.

Le Provost, C., Lyard, F., Molines, J.M., Genco, M.L. and Rabilloud, F. (1998) A hydrodynamic ocean tide model improved by assimilating a satellite altimeter-derived data set. *J. Geophys. Res.* **103**(C3)**:**5513–5529.

Logan, D.G. (1995) Oceanographic processes affecting larval transport in Beaufort Inlet, North Carolina. MSc Thesis, North Carolina State University, Raleigh, NC.

Luettich, R.A. Jr, Westerink, J.J. and Scheffner, N.W. (1992) ADCIRC: An advanced three-dimensional circulation model for shelves, coasts and estuaries; report 1: theory and methodology of ADCIRC-2DDI and ADCIRC-3DL. *Tech. Rep. DRP-92–6*. Coastal Engineering Research Center, US Army Engineer Waterways Experiment Station, Vicksburg, MS.

Luettich, R.A. Jr, Hench, J.L., Williams, C.D., Blanton, B.O. and Werner, F.E. (1998) Tidal circulation and larval transport through a barrier island inlet. In: *Estuarine and Coastal Modeling V*. M. Spalding *et al.* (eds). Reston, VA: ASCE, pp. 849–863.

Lynch, D.R., Werner, F.E., Greenberg, D.A. and Loder, J.W. (1992) Diagnostic model for baroclinic, wind-driven and tidal circulation in shallow seas, *Cont. Shelf Res.* **12:**37–64.

Mehta, A.J. and Joshi, P.B. (1988) Tidal inlet hydraulics. *J. Hydraul. Eng.* **114:**1321–1338.

Miller, J.M., Reed, J.P. and Pietrafesa, L.J. (1984) Patterns, mechanisms and approaches to the study of estuarine dependent fish larvae and juveniles. In: Mechanisms of Migration in Fishes. J.D. McCleave, G.P. Arnold, J.J. Dodson and W.H. Neill (eds.). New York: Plenum, pp. 209–225.

Ortel, G.F. (1988) Processes of sediment exchange between tidal inlets, ebb deltas and barrier islands. In: *Hydrodynamics and Sediment Dynamics of Tidal Inlets, Lecture Notes on Coastal and Estuarine Studies*, Vol. 29. D.G. Aubrey and L. Weishar (eds.). New York: Springer, pp. 297–318.

Pietrafesa, L.J. and Janowitz, G.S. (1988) Physical oceanographic processes affecting larval transport around and through North Carolina inlets. *Am. Fish Soc. Symp* **3:**34–50.

Power, J.H. (1997) Time and tide wait for no animal: seasonal and regional opportunities for tidal stream transport or retention, *Estuaries* **20**(2)**:**312–318.

Seaberg, W.C. (1988) Observations on inlet flow patterns derived from numerical and physical model studies. *Am. Fish Soc. Symp.* **3:**16–25.

Smith, N.P. and Stoner, A.W. (1993) Computer simulation of larval transport through tidal channels: role of vertical migration, *Estuar. Coast. Shelf Sci.* **37:**43–58.

Stegmann, P.M., Quinlan, J.A., Werner, F.E., Blanton, B.O. and Berrien, P. (1999) Atlantic menhaden recruitment to a southern estuary: defining potential spawning regions. *Fish. Oceanogr.* **8**(Suppl. 2):111–123.

Trinast, E.M. (1975) Tidal currents and *Acartia* distribution in Newport Bay, California. *Estuar. Coast. Mar. Sci.* **3:**165–176.

Werner, F.E., Blanton, B.O., Quinlan, J.A. and Luettich, R.A. Jr (1999) Physical oceanography of the North Carolina continental shelf during the fall and winter seasons: implications to the transport of larval menhaden. *Fish. Oceanogr.* **8**(Suppl. 2):7–21.

Wheless, G.H. and Valle-Levinson, A. (1996) A modeling study of tidally driven estuarine exchange through a narrow inlet onto a sloping shelf. *J. Geophys. Res.* **101**(C11)**:**25675–25687.

Zimmerman, J.T.F. (1976) Mixing and flushing of tidal embayments in the western Dutch Wadden Sea, part II: analysis of mixing processes, *Neth. J. Sea Res.* **10:**397–439.

Zimmerman, J.T.F. (1981) Dynamics, diffusion and geomorphological significance of tidal residual eddies. *Nature.* **290:**549–555.